International Journal of Research and Technology in Electrical Industry

journal homepage: ijrtei.sbu.ac.ir

Shahid Beheshti University

A Compact Ultra-Wideband Vivaldi Antenna with Parasitic Rings for mmWave 5G Applications

Hasan Falih Hamdan[1] , Mohammad Sajjad Bayati[1,*]

[1] *Department of Electrical Engineering, Razi University, Kermanshah, Iran*

ARTICLE INFO

Article history:
Received: 18 September 2025
Revised: 25 December 2025
Accepted: 29 December 2025

Keywords:
Ultra-wideband (UWB)
Vivaldi antenna
Parasitic rings
Millimeter-wave (mmWave)
5G communication

ABSTRACT

This paper introduces a compact, ultra-wideband Vivaldi antenna with parasitic elements, designed for 5G millimeter-wave (mmWave) applications. The antenna operates across a wide frequency range from 28.57 GHz to 80 GHz, covering essential high-frequency bands for current and future communication systems. The design features innovative elements such as curved circular flares and parasitic components, which boost both gain and directivity, thereby enhancing overall performance. The antenna is implemented on a Rogers RT5880 substrate with compact overall dimensions of 23 × 20 mm². Full-wave simulations using CST software show that the antenna achieves a peak gain of 10.5 dBi throughout the operating bandwidth and a radiation efficiency of up to 96%. To ensure impedance matching and reduce surface wave effects, a stepped-feedline is incorporated, promoting stable performance across the entire frequency range. The antenna exhibits desirable radiation characteristics, including low sidelobe levels and highly directional radiation patterns. With its compact size, high gain, and efficient operation, the antenna is well-suited for mmWave 5G communication systems, radar applications, and high-speed wireless networks.

1. Introduction

The need for high data rate, lower latency, and more connected devices has driven the rapid growth of millimeter-wave (mmWave) technology, especially for 5G and future wireless systems. Compared to systems that operate below 6 GHz, mmWave offers advantages like much wider bandwidth, better security, higher capacity, and improved resistance to interference [1-3]. However, to take advantage of these benefits, a larger bandwidth is needed, which is not available in the already crowded sub-6 GHz spectrum.

To address this, international regulatory organizations such as the World Radiocommunication Conference (WRC) and the International Telecommunication Union (ITU-R) have assigned mmWave bands, especially those above 24 GHz, for next-generation wireless services [4, 5]. Notably, frequency bands centered at 28 GHz, 38 GHz, the unlicensed 60 GHz (WiGig), and the E-band (71–86 GHz) have become key candidates for both licensed and unlicensed 5G applications [6, 7].

With these advancements, antenna designers are challenged to develop compact, high-performance, and cost-effective antenna systems capable of operating reliably over wide frequency ranges while maintaining consistent radiation characteristics. Among wideband antenna structures, the Vivaldi antenna (VA) proposed initially by Gibson in 1979 [8] stands out due to its inherent ultra-wideband behavior, high gain, low profile, and ease of fabrication [9, 10]. These features make it an excellent candidate for mmWave systems supporting applications such as automotive radar, satellite communications, wearable devices, and high-speed indoor wireless networks [11-13].

* Corresponding author
E-mail address: s.bayati@razi.ac.ir
https://orcid.org/0000-0002-5184-8840
https://doi.org/10.48308/ijrtei.2026.241594.1102

Early research on 5G mmWave antennas focused on wideband microstrip patch antennas due to their ease of fabrication and integration. Reference [14] introduced a Y-shaped patch antenna, achieving a narrow bandwidth (27.5–28.25 GHz) with a 7.6 dBi gain. In [15] performance was improved with the use of a slot and elliptical patch antenna, broadening the bandwidth to 26.4 –31.6 GHz with 8 dBi gain, although with reduced efficiency (80%). To improve impedance matching and gain, helical-inspired and slot-loaded antennas were proposed. In [16] a helical-inspired patch antenna was developed, exhibiting a gain of 5.9 dBi within the frequency range of 26–29 GHz, while [17] presented a slot-loaded rectangular patch antenna that attained an 8.2 dBi gain and 91.66% efficiency throughout the frequency range of 26.6–29 GHz. Despite these improvements, traditional microstrip structures have challenges in achieving ultra-wideband performance over 30 GHz.

Recent designs are intended to cover several 5G bands by broadening bandwidth coverage. Reference [18] introduced a rectangular box-type antenna functioning throughout the frequency range of 23.5–65 GHz, with a gain of 5.66 dBi and an efficiency of 93%. In [19] multi-band coverage was further enhanced via a quasi-Yagi antenna on an LCP substrate, attaining a bandwidth of 24–71 GHz but with a 70% radiation efficiency. Compact multi-band solutions were also explored. A rectangular monopole antenna was introduced in [20], covering 6.24–13.89 GHz with a peak gain of 10.75 dBi, whereas [21] proposed a flower-shaped wideband antenna, achieving 3.7–60 GHz bandwidth with 96% efficiency. However, these solutions often face limitations in directivity and radiation performance at higher mmWave frequencies.

Several Vivaldi antenna designs have been extensively explored in literature, each demonstrating varying levels of bandwidth and gain, tailored to meet the demanding specifications of mmWave 5G communication systems. A printed UWB Vivaldi antenna utilizing a stepped slotline-to-tapered patch transition achieved a bandwidth of 3–15.1 GHz and a gain of 8.2 dBi [22]. while a planar slotted meander-line antipodal Vivaldi antenna covered a narrower band of 25–30 GHz, with a gain of 6.7 dBi[23]. Noteworthy advancements include a Chebyshev-tapered antipodal Vivaldi antenna, which broadened the operational bandwidth from 1 to 35 GHz, achieving a gain of 6.8 dBi [24]. Additionally, a Vivaldi antenna with asymmetric parasitic patches operated from 6 GHz to 26.5 GHz, providing a 9 dBi gain [25]. As well as a fractal-shaped dielectric slab-based antenna offering a broad 4.2–50 GHz bandwidth, though without specified gain [26]. Dual-polarized versions have extended the range from 22.5 to 45 GHz, with gain values between 5.5 and 8.5 dBi [27], while a miniaturized design using metallic vias and directors achieved 16.5–36.6 GHz with a peak gain of 11.9 dBi [28]. Another innovative design incorporated sun-shaped rectangular slits, extending the bandwidth to 5–50 GHz with a gain of 10 dBi [29].

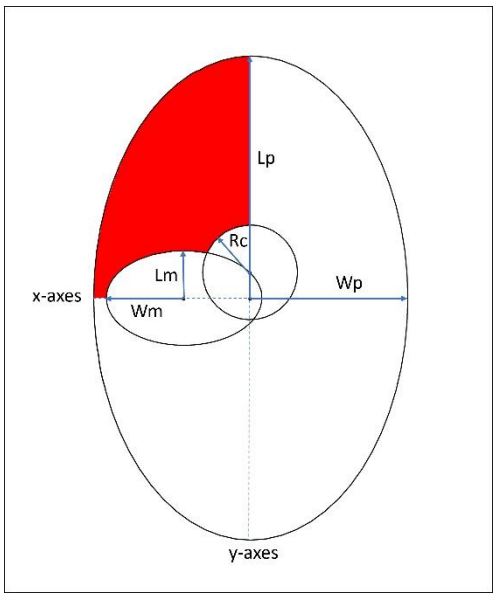

Fig. 1. Geometrical construction of the antenna arms

Metamaterial-enhanced designs, such as the metamaterial-slab-loaded antipodal Vivaldi antenna, expanded the operational range from 3.68 to 43.5 GHz with a gain of 10 dBi [30].

Among the highest-performing designs, a log-periodic slot-loaded circular Vivaldi antenna achieved a bandwidth from 5 to 40 GHz with a maximum gain of 12 dBi [31]. Despite these innovations, there remains a design gap in achieving a compact Vivaldi antenna structure that can operate across the high mmWave spectrum with stable gain, high efficiency, and robust directivity. Most prior works either lack sufficient gain at higher frequencies, suffer from large size, or require complex fabrication processes.

This paper introduces a novel mmWave Vivaldi antenna that combines a compact elliptical-tapered flare with parasitic rings to enhance gain, bandwidth, and radiation stability. Unlike traditional exponential or Chebyshev taper profiles, the design employs the geometric intersection of ellipses to achieve a smooth impedance transition and reduce aperture size. Parasitic rings near the arms improve end-fire directivity. Simulation results show that the antenna operates over an ultra-wide band from 28.57 to 80 GHz with more than 92% radiation efficiency and a peak gain of 10.5 dBi, making it a promising candidate for future 5G and beyond communication systems.

2. Design and Structure of the Proposed Vivaldi Antenna

The suggested antenna design comprises three layers: a radiating patch, a dielectric substrate, and a ground plane, as seen in Fig 1. The radiating patch, printed on the top layer, is the main radiating element, with the ground plane at the bottom.

A dielectric substrate is layered between these layers, providing mechanical support and influencing the antenna's electromagnetic characteristics. The proposed antenna appears as a radiating slot that progressively expands from the feed point. The dual conductive arms,

constructed on both surfaces of the dielectric substrate, establish the radiating structure. In contrast to an ideal infinite extension, the arms are limited to a finite length for practical application, resulting in a configuration similar to a coplanar waveguide.

Each arm of the antenna is designed using a systematic geometrical approach based on the combination of two ellipses and a circular section, as shown in Fig 1. The first ellipse is oriented vertically, defined by its major radius (Lp=10.35 mm) along the y-axis and its minor radius (Wp=6.7 mm) along the x-axis. The second ellipse, smaller and oriented horizontally, has its major radius (Wm=3.3 mm) along the x-axis and its minor radius (Lm=2 mm) along the y-axis, positioned so that its major axis aligns with the minor axis of the first ellipse. Additionally, a circular element with radius (Rc=2 mm) is included near the center of the vertical ellipse, intersecting with the horizontal ellipse to form the arm structure. One radiating arm is located on the top layer and connected to the feed line of the antenna, while the other arm is placed on the bottom layer and connected to the ground plane.

The proposed antenna is excited through a 50-Ω microstrip feed line printed on a Rogers RT5880 substrate. The initial width of the microstrip line was determined using classical closed-form transmission-line equations to achieve the required characteristic impedance [32]. The effective dielectric constant ε_{eff} of the microstrip line is given by:

$$\varepsilon_{eff} = \frac{\varepsilon_r+1}{2} + \frac{\varepsilon_r-1}{2}\left(1+12\frac{h}{w}\right)^{-\frac{1}{2}} \qquad (1)$$

where εr is the relative permittivity of the substrate, h is the substrate thickness, and W is the width of the microstrip feed line.For microstrip lines with a width-to-height ratio W/h>1, the characteristic impedance Z_0 can be approximated by:

$$z_0 = \frac{120\pi}{\sqrt{\varepsilon_{eff}}\left(\frac{w}{h}+1.393+0.667\ln\left(\frac{w}{h}+1.444\right)\right)} \qquad (2)$$

To further improve impedance matching between the antenna input and the standard 50-Ω source, a stepped-impedance microstrip feeding network is employed. This configuration enables gradual impedance transformation, thereby enhancing power transfer and minimizing reflection across the operating frequency band. As shown in Fig 2, the line starts with an initial width of 0.72 mm (denoted as wf1) and gradually tapers in discrete steps along the length. Each step has a uniform length of 1 mm, with the widths decreasing successively to 0.62 mm (wf2), 0.58 mm (wf3), 0.52 mm (wf4), and finally 0.40 mm (wf5). This thin stepped-impedance microstrip feed line is employed to provide a gradual reduction in conductor width, enabling a smooth impedance transition between the feed line and the radiating arms. This gradual transition significantly improves impedance matching, reduces reflection losses, and enhances the overall radiation performance of the antenna, which is particularly critical for stable operation at millimeter-wave frequencies.

To enhance the performance of the proposed antenna, three concentric parasitic resonant rings with radius R1=0.75 mm, R2=1.2 mm, and R3=2.3 mm were added to the top radiating arm. These rings are not directly connected to the feed line and operate through electromagnetic coupling with the main radiating element. Their presence creates additional resonant paths on the upper arm, which improves the surface current distribution and increases radiation at the target frequencies. Although their effect on the antenna's input impedance is limited and indirect, the rings are essential in expanding the operational bandwidth, enhancing impedance matching at the resonant frequencies, and boosting radiation gain. Incorporating these parasitic elements provides an effective way to optimize overall antenna performance without changing the main antenna structure.

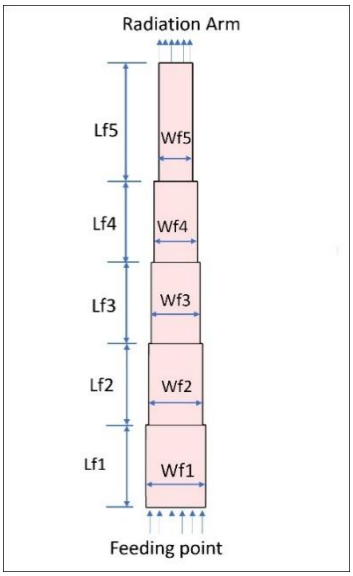

Fig. 2. Structure of the proposed antenna's feeding network using a stepped-impedance microstrip line

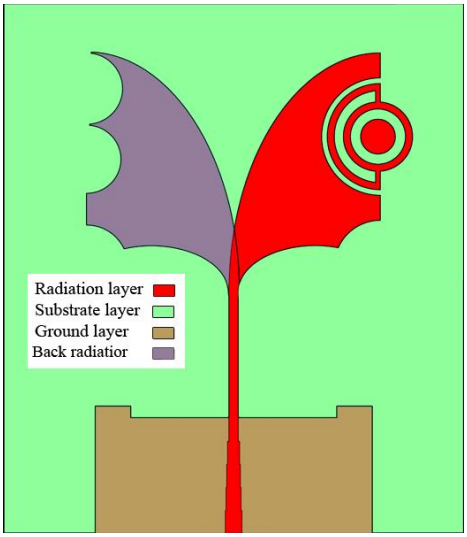

Fig. 3. Geometry of the proposed Vivaldi antenna

The bottom layer of the antenna, the lower arm, was modified by semicircular holes with different radii, namely Rg1=1.57 mm and Rg2=1.5 mm. semicircular holes were used instead of rectangular or sharp-edged structures to achieve a smoother distribution of surface currents, which helps reduce field concentration and scattering losses at the edges. The curved geometry of

these semicircle holes also creates additional resonant paths within the antenna, enhancing its frequency response and broadening the bandwidth. After these modifications, the lower arm was directly connected to the ground plane, which is rectangular with dimensions Wg=12 mm and Lg=5.5 mm. This configuration provides a stable electrical reference, improves impedance matching, and stabilizes the radiation pattern.

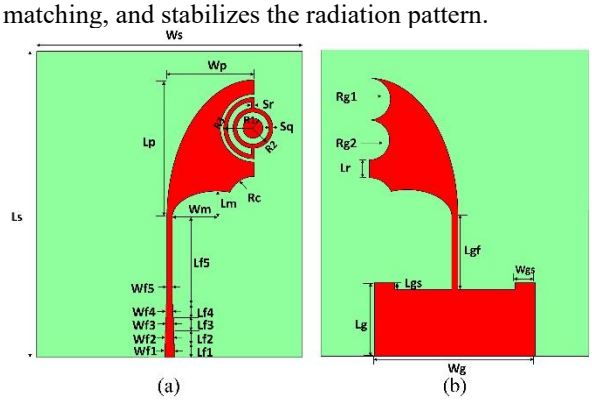

Fig. 4. Detailed structural dimensions of the antenna. (a) Top layer, (b) Bottom with Ground layer

Combining these holes with the direct ground connection allows for better control of the antenna's characteristics and increases its efficiency over a wide range of frequencies. Fig 3 shows the complete geometry of the proposed Vivaldi antenna, depicting the final design after modifications.

The dielectric substrate used in the proposed design is Rogers RT/duroid 5880, with a relative permittivity is εr=2.2 and the thickness equals to 0.254 mm, the width and length of the substrate were Ws=20 mm and Ls=23 mm, respectively.

This material was chosen because of its exceptionally low dielectric constant, which allows for wider bandwidth and reduces surface wave losses, thus improving the antenna's radiation efficiency. Additionally, it's very low loss tangent ($\tan\delta \approx 0.0009$). lowers dielectric losses, making it very suitable for high-frequency and millimeter-wave applications. The substrate thickness offers an ideal balance between mechanical stability and electromagnetic performance: a thinner substrate suppresses higher-order modes and spurious radiation while still providing sufficient structural rigidity.

Fig 4 illustrates the main structural parameters such as the radiation arms, ground plane, and feed region. The design was optimized using a structured parametric approach. Key geometrical parameters were systematically varied to study their influence on impedance matching and gain. The final design represents a global optimization that provides stable ultra-wideband performance across the entire operating frequency range. All geometric parameter values are listed in Table 1, providing a detailed reference for the antenna dimensions used in simulation and performance assessment.

3. Simulation results of the proposed antenna

The proposed antenna design was assessed using CST Microwave Studio 2018, a full-wave electromagnetic simulation tool. The simulation involved exciting the antenna with a discrete port connected to the feed line. The results shown here, such as return loss, impedance bandwidth, radiation patterns, and gain, were directly obtained from these simulations and are used to confirm the design's effectiveness.

Table 1: Optimized dimensions of the proposed Vivaldi antenna (unit: mm)

Dimension	Value	Dimension	Value
Ws	20	***R1***	0.75
Ls	23	***R2***	1.5
Wf1	0.72	***R3***	2.3
Wf2	0.65	***Wg***	12
Wf3	0.58	***Lg***	5.5
Wf4	0.52	***Lgf***	5.5
Wf5	0.4	***Wgs***	1.5
Lf1, Lf2, Lf3, Lf4	1.0	***Lgs***	0.5
Lf5	6.0	***Lr***	1.33
Wp	6.6	***Wg1***	1.57
Lp	10.36	***Wg2***	1.5
Lm	2.0	***Sr***	0.2
Wm	3.3	***Sq***	0.3
Rc	2.0	**h**	0.254

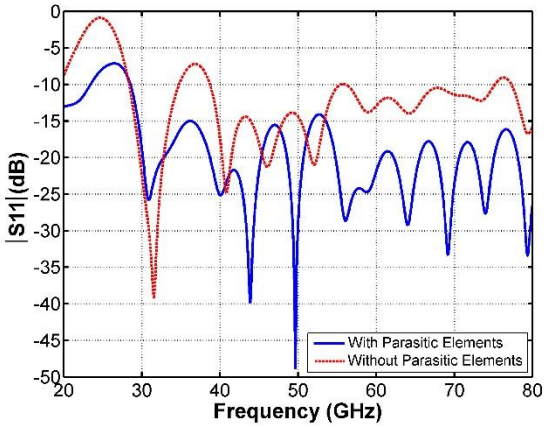

Fig. 5. Return loss results or the proposed antenna

Fig 5 displays the simulated return loss ($|S_{11}|$) of the proposed antenna. The results show that the antenna maintains very low return loss values throughout the operating range, confirming excellent impedance matching between the feed network and the radiating structure. Notably, the lowest return losses occur at 43.88 GHz (-39.8 dB) and 49.64 GHz (-48.6 dB), indicating high power transfer efficiency and minimal reflection. These deep resonances are primarily due to the smooth taper of the antenna arms and the optimized feed transition, which effectively reduce unwanted reflections. These findings emphasize the antenna's capability to operate with high radiation efficiency and stability within the targeted frequency range.

Fig 6 shows the simulated VSWR of the proposed antenna, which remains close to unity across the entire frequency range, indicating excellent impedance matching. The lowest VSWR of 1.00 occurs at 49.64 GHz, confirming near-perfect matching at this point. This

outstanding performance is mainly due to the stepped and gradually tapered feed network, which provides a smooth impedance transition.

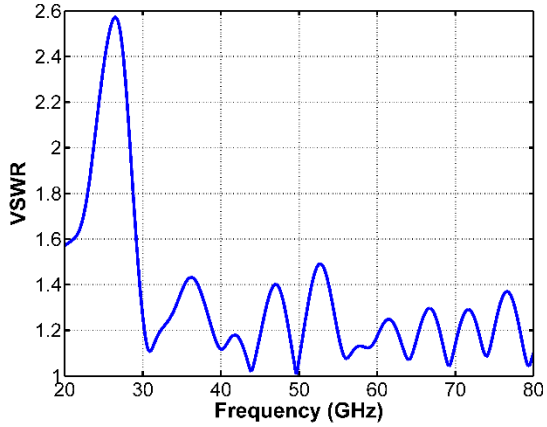

Fig. 6. VSWR results of the proposed antenna

By reducing the feed line width gradually, impedance discontinuities and reflections are minimized, resulting in stable broadband matching and efficient power transfer throughout the operating band.

The antenna shows excellent total and radiation efficiency at all simulated frequencies, as illustrated in Fig 7. A maximum efficiency of 96.2% occurs at 31 GHz, with efficiency remaining consistently above 92% throughout the entire operating range. This high efficiency is mainly due to the antenna's traveling-wave structure, which evenly distributes current along the extended arms and reduces unwanted surface wave effects. Additionally, using a low-loss Rogers RT/duroid 5880 substrate minimizes dielectric losses and surface waves.

As shown in Fig 8, the proposed antenna demonstrates stable high-gain performance, ranging from 9.8 dBi at 31 GHz to 10.5 dBi at 79.34 GHz. This consistently high gain is mainly due to the extended flare length and the gradual expansion of the radiating arms, which effectively increase the radiation aperture and support strong end-fire directivity. As a result, the antenna maintains broadband high-gain radiation.

To thoroughly evaluate the performance of the proposed antenna, both two-dimensional and three-dimensional far-field radiation patterns were examined at the resonant frequencies of 31 GHz, 56.06 GHz, 64.04 GHz, and 79.34 GHz, as shown in Figures 9 and 10. These frequencies were carefully chosen because they correspond to the points of lowest return loss while covering the entire ultra-wideband operating range. The inclusion of parasitic resonant rings in the antenna design was essential in maintaining stable radiation characteristics across the broadband spectrum. At 31 GHz, the radiation patterns in both the E-plane and H-plane show strong directivity, with a main lobe gain of 9.84 dB and low side lobe levels.

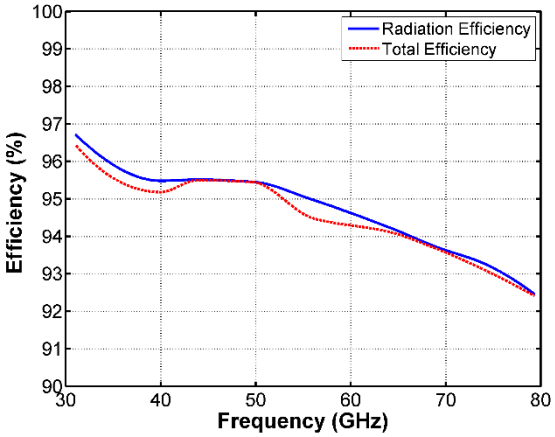

Fig. 7. Efficiency results of the antenna

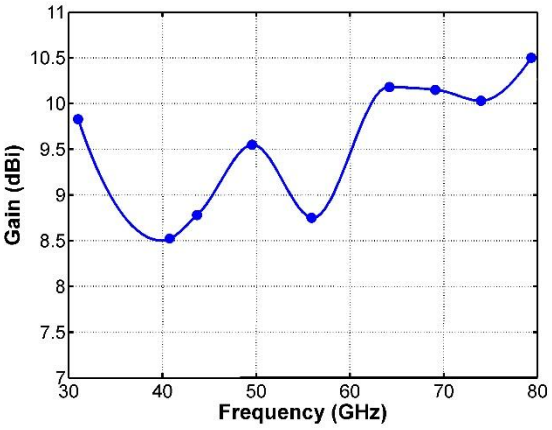

Fig. 8. Gain results of the proposed antenna

The high performance results from the optimized antenna shape combined with parasitic rings, which generate additional resonant modes, enhancing impedance matching and enabling stable broadband operation. At 56.06 GHz, the main lobe slightly decreases to 8.31 dB, while low side lobes remain, confirming robust directional performance. As the frequency increases to 64.04 GHz, the main lobe gain improves to 8.88 dB, further increasing directivity. At the upper end of the operating band, at 79.34 GHz, the antenna maintains a narrow beam with a main lobe gain of 8.68 dB, demonstrating its ability to sustain steady radiation across a wide frequency range.

Overall, the proposed Vivaldi antenna, enhanced with parasitic resonant rings, delivers stable radiation patterns, high gain, and low side lobes across its ultra-wideband spectrum. These qualities make the design especially suitable for next-generation mmWave applications such as 5G, where precise beam steering, efficient end-fire radiation, and reliable wideband performance are critical.

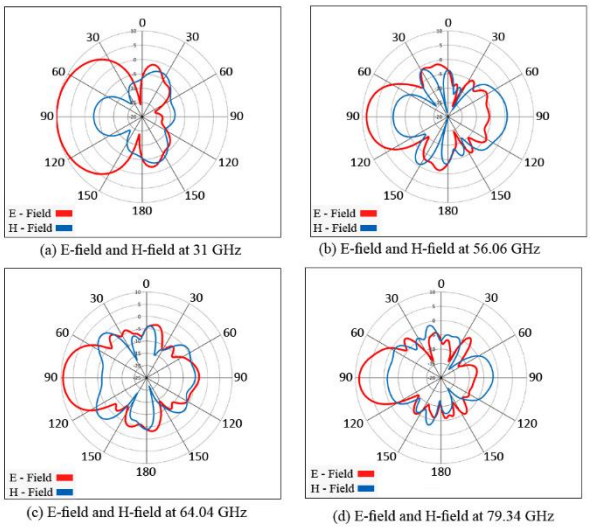

(a) E-field and H-field at 31 GHz (b) E-field and H-field at 56.06 GHz

(c) E-field and H-field at 64.04 GHz (d) E-field and H-field at 79.34 GHz

Fig. 9. Far field results of the antenna in the 2D form at various frequencies.

Additionally, the surface current distribution of the proposed antenna at resonant frequencies was analyzed to better understand the radiation mechanism. As shown in Fig 11, the highest current densities are concentrated along the edges of the radiating arms and gradually decrease toward their centers. A noticeable concentration of surface currents is also present around the regions between the parasitic rings and the main radiating arm. This behavior highlights the strong electromagnetic coupling between the parasitic elements and the main radiator. The parasitic rings effectively redistribute the surface currents, creating additional resonant pathways that enhance radiation efficiency and directivity. This redistribution helps confine the radiated fields more tightly along the final firing direction and results in a significant gain increase, especially at higher frequencies within the operating range. The analysis confirms that adding parasitic rings also improves the radiation characteristics, making the design highly suitable for high-frequency and millimeter-wave applications.

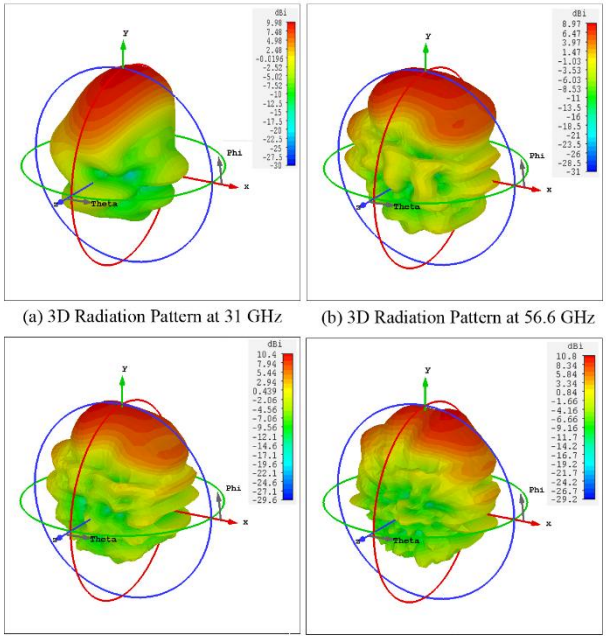

(a) 3D Radiation Pattern at 31 GHz (b) 3D Radiation Pattern at 56.6 GHz

(c) 3D Radiation Pattern at 64.04 GHz (d) 3D Radiation Pattern at 79.34 GHz

Fig. 10. Far-field results of the antenna in the 3D form at various frequencies

4. Parametric Analysis

A parametric analysis of the proposed design was conducted to evaluate the robustness of the proposed design compared to realistic manufacturing tolerances. The analysis involved varying the values of the main antenna dimensions and evaluating the impact on return loss (|S11|) and achieved gain. Experimental validation was not conducted due to the unavailability of local fabrication and millimeter-wave measurement facilities operating up to 80 GHz. Therefore, this simulation-based analysis was conducted to validate the design and its overall performance. During the parametric analysis, the fundamental antenna dimensions were systematically varied. These included the dimensions of the first elliptical section (Wp and Lp), the second elliptical section (Wm and Lm), the diameter of the circular element (Rc), the feed parameters (Wf1 and Wf5), and the radius of the middle parasitic ring (R2).

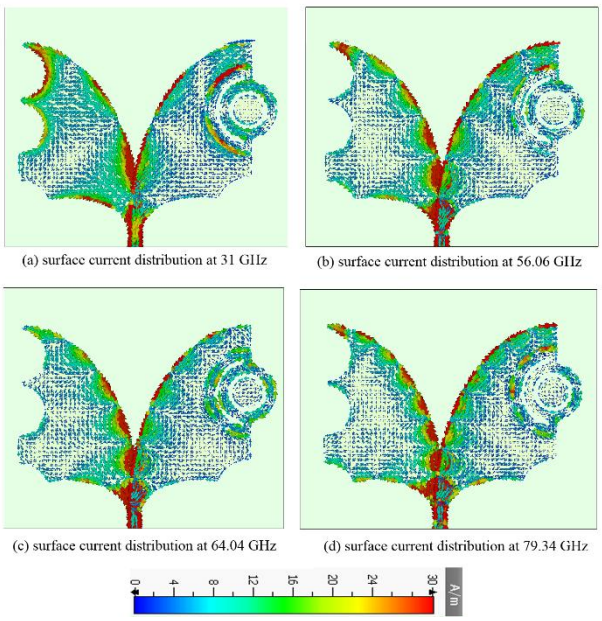

Fig 11. Surface current distribution at resonance frequencies

Table 2. Considered dimensional variations of the antenna structure

Parameter	Baseline (mm)	-Δ (mm)	+Δ(mm)
Wp	6.6	6.4	6.8
Lp	10.36	10.16	10.56
Wm	3.30	3.15	3.45
Lm	2.00	1.80	2.20
Rc	2.00	1.80	2.20
Wf1	0.72	0.52	0.92
Wf5	0.40	0.38	0.42
R2	1.50	1.30	1.70

For each parameter, three values were evaluated: the nominal (baseline) value, a lower deviation (−Δ), and an upper deviation (+Δ), corresponding to typical manufacturing tolerances. The baseline, lower, and upper values are summarized in Table 2.

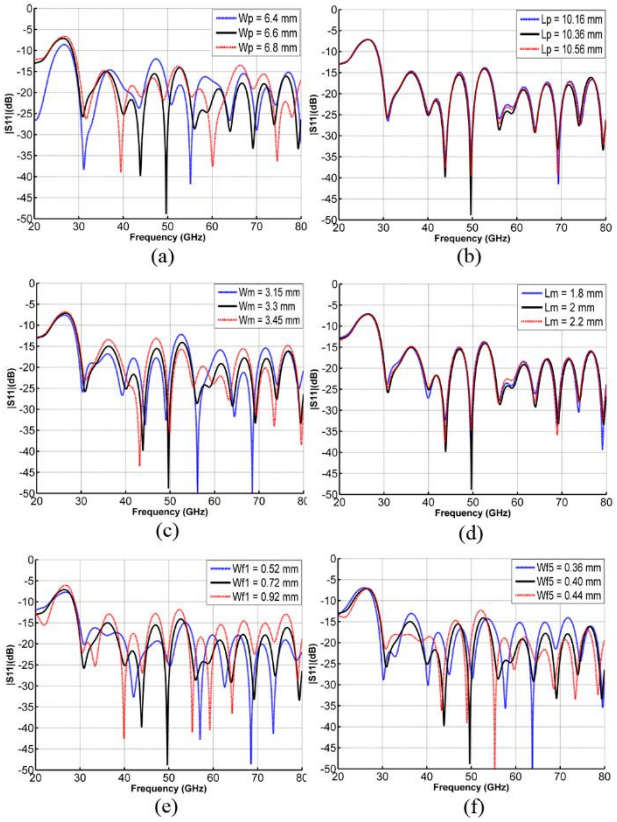

Fig. 12. Return loss results for different values of (a) Wp, (b) Lp, (c) Wm, (d) Lm, (e) Wf1, and (f) Wf5.

The analysis results shown in Figures 12 and 13 indicate that small variations in the first elliptical geometry (Wp and Lp) cause minor shifts in the lower band edge and resonance minima, but the antenna's ultra-wideband performance remains consistent across all tested values. Changes in the second elliptical geometry (Wm and Lm) result in slight resonance adjustments with little effect on impedance matching. Variations in the final feed width Wf5 are most noticeable at higher frequencies, causing controlled variations in |S11| and a slight spread in gain. Modifications to the middle parasitic ring radius R2 slightly affect gain but do not compromise radiation patterns, indicating that parasitic tuning can be performed without degrading overall performance. These results demonstrate that the antenna design is robust against small fabrication variations, and the simulation suggests it will function as intended under normal manufacturing conditions.

5. Comparison with Previous Works

Table 3 compares the proposed antenna with earlier designs, focusing on size, operating bandwidth, fractional bandwidth, peak gain, and design approach. The analysis highlights the unique benefits of the proposed two-arm Vivaldi antenna with parasitic rings.

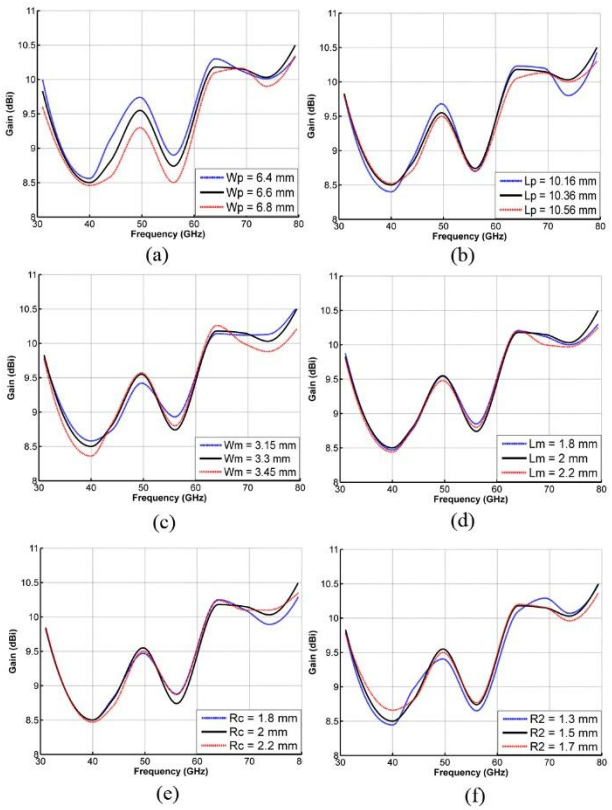

Fig. 13. Gain results for various values of (a) Wp, (b) Lp, (c) Wm, (d) Lm, (e) Rc, and (f) R2.

It is clear that this design achieves the broadest bandwidth, ranging from 28.57 to 80 GHz (51.43 GHz), outperforming all previous work. While some designs show higher fractional bandwidths over 160%, they are based on much lower centre frequencies, leading to smaller usable spans in the millimeter-wave range. For emerging 5G and future applications, full coverage of the mmWave spectrum is a vital benchmark, and in this regard, the proposed antenna offers clear advantages. Regarding size, the proposed structure is more compact than several existing designs, such as [22, 25], which is highly beneficial for contemporary integrated communication systems. In terms of gain, the proposed antenna performs better than many earlier studies. Although certain designs, such as [26, 28, 31], demonstrate higher gains, they are characterized by larger physical dimensions and narrower bandwidths. The superior gain of this antenna is attributed to the extended flare length and the inclusion of parasitic rings, which enhance the effective aperture and improve end-fire directivity throughout the entire frequency band. Overall, the proposed Vivaldi antenna effectively balances key performance metrics in comparison to other studies. These features make it as a promising candidate for next-generation mmwave and 5G communication systems.

Table 3. Comparison of the proposed antenna with other previous Vivaldi antennas

Ref. no	Size (mm^3)	BW (GHz)	FB (%)	Peak gain (dBi)	Design methodology
[22]	41 ×48 ×0.8	3 - 15.1	134 %	8.2	Stepped slotline tapered patch
[23]	50 × 20 × 1.6	25 - 30	18%	6.7	Slotted meander-line
[24]	100 × 100 × 1.6	1 - 35	189%	6.8	Chebyshev tapering
[25]	124 × 66 × 1.575	6 - 26.5	127%	9	Asymmetric parasitic patches
[26]	122 × 66 × 1.524	4.2 - 50	169.8%	16.9	Fractal dielectric slab
[27]	12 × 5.5 × 0.254	22.5 - 45	66.67%	8.5	Tapered Slot Antenna
[28]	30.4 ×30.4 × 0.787	16.5 - 36.6	71.24%	11.9	Metallic vias & directors
[29]	30×55×0.508	5-50	163.6%.	10	Sun-shaped slits
[30]	60 × 40 × 0.508	3.68–43.5	169%	>10	Metamaterial slab loading
[31]	45 × 60 × 0.762	5 - 40	155.56%	12	Log-periodic slot-loaded circular
This work	20 × 23 × 0.254	28.57-80	93.5%	10.5	Two-arm Vivaldi with parasitic rings

6. Conclusion

This paper introduces a new Vivaldi antenna design optimized for ultra-wideband millimeter-wave applications. It features a novel arm construction method utilizing the intersection of two ellipses and a single circle to form a compact, efficient radiation structure. The antenna is built on a Rogers RT5580 substrate with a stepped-impedance microstrip line, ensuring broad-frequency impedance matching. To improve radiation, parasitic ring elements are added near the flare arms, enhancing overall performance. Simulation results indicate the antenna operates from 28.57 GHz to 80 GHz, with a return loss better than −25 dB across the entire bandwidth, a peak gain of 10.5 dBi, and radiation efficiency over 92%. The far-field patterns demonstrate directional end-fire radiation, ideal for mmWave applications. Its compact size, high efficiency, and straightforward fabrication make it a promising choice for integration into next-generation 5G, radar, and high-speed wireless networks.

7. References

[1] X. Wang et al., “Millimeter wave communication: A comprehensive survey,” IEEE Communications Surveys & Tutorials, vol. 20, no. 3, pp. 1616–1653, 2018.

[2] L. Tsai and W. Chen, “A UWB antenna with band‐notched filters using slot‐type split ring resonators,” Microw Opt Technol Lett, vol. 58, no. 11, pp. 2595–2598, 2016.
[3] W. M. Abdulkawi, W. A. Malik, A. A. Sheta, and M. A. Alkanhal, “A compact dual circular patch pattern reconfigurable antenna,” Microw Opt Technol Lett, vol. 60, no. 11, pp. 2762–2768, 2018.
[4] W. Roh et al., “Millimeter-wave beamforming as an enabling technology for 5G cellular communications: Theoretical feasibility and prototype results,” IEEE communications magazine, vol. 52, no. 2, pp. 106–113, 2014.
[5] Y. You, Y. Lu, T. Skaik, Y. Wang, and J. Huang, “Millimeter-wave 45° linearly polarized corporate-fed slot array antenna with low profile and reduced complexity,” IEEE Trans Antennas Propag, vol. 69, no. 9, pp. 6064–6069, 2021.
[6] W. A. Awan, “Tiny form factor with ultra wide band rectangular patch antenna for 5G applications,” in 2018 International Conference on Computing, Mathematics and Engineering Technologies (iCoMET), IEEE, 2018, pp. 1–4.
[7] C. J. Hansen, “WiGiG: Multi-gigabit wireless communications in the 60 GHz band,” IEEE Wirel Commun, vol. 18, no. 6, pp. 6–7, 2011.
[8] P. J. Gibson, “The vivaldi aerial,” in 1979 9th European Microwave Conference, IEEE, 1979, pp. 101–105.
[9] J. Wu, Z. Zhao, Z. Nie, and Q.-H. Liu, “A printed UWB Vivaldi antenna using stepped connection structure between slotline and tapered patches,” IEEE Antennas Wirel Propag Lett, vol. 13, pp. 698–701, 2014.
[10] K. Muzaffar, M. I. Magray, G. S. Karthikeya, and S. K. Koul, “High gain broadband Vivaldi antenna for 5G applications,” in 2019 International Conference on Electromagnetics in Advanced Applications (ICEAA), IEEE, 2019, pp. 496–497.
[11] M. Awais, A. Riaz, and W. T. Khan, “An ultra-wideband (16 40 GHz) mmWave antenna for automotive radar and 5G applications,” in 2019 IEEE International Symposium on Antennas and Propagation and USNC-URSI Radio Science Meeting, IEEE, 2019, pp. 1919–1920.
[12] N. R. Palepu and J. Kumar, “Neutralized meander line patch antipodal vivaldi defected ground millimeter-wave (mm-wave) antenna array,” AEU-International Journal of Electronics and Communications, vol. 166, p. 154663, 2023.
[13] L. Song, B. Zhang, D. Zhang, and Y. Rahmat-Samii, “Embroidery electro-textile patch antenna modeling and optimization strategies with improved accuracy and efficiency,” IEEE Trans Antennas Propag, vol. 70, no. 8, pp. 6388–6400, 2022.
[14] W. A. Awan, A. Zaidi, and A. Baghdad, “Patch antenna with improved performance using DGS for 28GHz applications,” in 2019 international conference on wireless technologies, embedded and intelligent systems (WITS), IEEE, 2019, pp. 1–4.
[15] H. Zahra, M. Hussain, S. Shrestha, M. Asadnia, S. M. Abbas, and S. Mukhopadhyay, “Printed planar antenna for 28GHz 5G millimeter wave applications,” in 2022 IEEE International Symposium on Antennas and Propagation and USNC-URSI Radio Science Meeting (AP-S/URSI), IEEE, 2022, pp. 53–54.
[16] H. Zahra, W. A. Awan, W. A. E. Ali, N. Hussain, S. M. Abbas, and S. Mukhopadhyay, “A 28 GHz broadband helical inspired end-fire antenna and its MIMO configuration for 5G pattern diversity applications,” Electronics (Basel), vol. 10, no. 4, p. 405, 2021.
[17] A. D. Tadesse, O. P. Acharya, and S. Sahu, “A compact planar four-port MIMO antenna for 28/38 GHz millimeter-wave 5G applications,” Advanced Electromagnetics, vol. 11, no. 3, pp. 16–25, 2022.
[18] A. Jabbar, M. A. Imran, Q. H. Abbasi, and M. U. Rehman, “Design of a Compact Ultra-Wideband Microstrip Antenna for Millimeter-Wave Communication,” in 2021 IEEE International Symposium on Antennas and Propagation and USNC-URSI Radio Science Meeting (APS/URSI), IEEE, 2021, pp. 837–838.
[19] B. Lyu, G. A. Safdar, M. A. Jamshed, and M. Ur-Rehman, “Flexible Ultra-Wideband Antenna for 5G and Beyond Wearable Applications,” in 2021 1st International Conference on Microwave, Antennas & Circuits (ICMAC), IEEE, 2021, pp. 1–4.
[20] S. Salagrama, S. K. Pittala, K. Sharma, G. P. Pandey, N. K. U. Pande, and D. K. Singh, “Ultrawideband printed monopole antenna for X band and 5G applications,” in 2022 International Conference on Computational Intelligence and Sustainable Engineering Solutions (CISES), IEEE, 2022, pp. 251–255.
[21] S. Gaur, D. Lodhi, S. Singhal, and M. Salim, “Compact flower shape super wideband antenna for mmWave applications,” in 2022 URSI Regional Conference on Radio Science (USRI-RCRS), IEEE, 2022, pp. 1–4.
[22] J. Wu, Z. Zhao, Z. Nie, and Q.-H. Liu, “A printed UWB Vivaldi antenna using stepped connection structure between slotline and tapered patches,” IEEE Antennas Wirel Propag Lett, vol. 13, pp. 698–701, 2014.
[23] N. R. Palepu, J. Kumar, S. Peddakrishna, and A. Ghosh, “Wideband meander-line-antipodal-Vivaldi slot-antenna for millimeter-wave applications,” e-Prime-Advances in Electrical Engineering, Electronics and Energy, vol. 9, p. 100641, 2024.
[24] A. Gorai, A. Karmakar, M. Pal, and R. Ghatak, “A super wideband Chebyshev tapered antipodal Vivaldi antenna,” AEU-International Journal of Electronics and Communications, vol. 69, no. 9, pp. 1328–1333, 2015.
[25] J. Bang, J. Lee, and J. Choi, “Design of a wideband antipodal Vivaldi antenna with an asymmetric parasitic patch,” Journal of Electromagnetic Engineering and Science, vol. 18, no. 1, pp. 29–34, 2018.
[26] A. Bhattacharjee, A. Bhawal, A. Karmakar, and A. Saha, “Design of an antipodal Vivaldi antenna with fractal‐shaped dielectric slab for enhanced radiation characteristics,” Microw Opt Technol Lett, vol. 62, no. 5, pp. 2066–2074, 2020.
[27] A. Azari, A. Skrivervik, H. Aliakbarian, and R. A. Sadeghzadeh, “A super wideband dual-polarized vivaldi antenna for 5G mmWave applications,” Ieee Access, vol. 11, pp. 80761–80768, 2023.
[28] J. Li, J. Huang, H. He, and Y. Wang, “A high-gain Metallic-via-loaded antipodal vivaldi antenna for millimeter-wave application,” Electronics (Basel), vol. 13, no. 10, p. 1898, 2024.
[29] M. Moosazadeh, S. Kharkovsky, J. T. Case, and B. Samali, “Improved radiation characteristics of small antipodal Vivaldi antenna for microwave and millimeter-wave imaging applications,” IEEE Antennas Wirel Propag Lett, vol. 16, pp. 1961–1964, 2017.
[30] X. Li, H. Zhou, Z. Gao, H. Wang, and G. Lv, “Metamaterial slabs covered UWB antipodal Vivaldi antenna,” IEEE Antennas Wirel Propag Lett, vol. 16, pp. 2943–2946, 2017.
[31] W. Mazhar, D. Klymyshyn, and A. Qureshi, “Log periodic slot‐loaded circular vivaldi antenna for 5-40 GHz UWB applications,” Microw Opt Technol Lett, vol. 59, no. 1, pp. 159–163, 2017.
[32] Pozar, David M. "Microwave engineering." Fourth Editions, University of Massachusetts at Amherst, John Wiley & Sons, Inc (2012): 26-3